

Article

Structure and Activity of Ni₂P/Desilicated Zeolite β Catalysts for Hydrocracking of Pyrolysis Fuel Oil into Benzene, Toluene, and Xylene

Yong-Su Kim, Kye-Sung Cho and Yong-Kul Lee * 

Laboratory of Advanced Catalysis for Energy and Environment, Department of Chemical Engineering, Dankook University, 152 Jukjeonro, Yongin 16890, Korea; nakimys@gmail.com (Y.-S.K.); ssamjangcks@naver.com (K.-S.C.)

* Correspondence: yolee@dankook.ac.kr; Tel.: +82-31-8005-3466

Received: 6 December 2019; Accepted: 25 December 2019; Published: 01 January 2020



Abstract: The effects of desilication (DS) of the zeolite β on the hydrocracking of polycyclic aromatics were investigated using the Ni₂P/β catalysts. The Ni₂P/β catalysts were obtained by the temperature-programmed reduction (TPR) method, and the physical and chemical properties were examined by N₂ physisorption, X-ray diffraction (XRD), ²⁷Al magic angle spinning–nuclear magnetic resonance (²⁷Al MAS NMR), extended X-ray absorption fine structure (EXAFS), isopropyl amine (IPA) and NH₃ temperature-programmed desorption (TPD), CO uptake, and thermogravimetric analysis (TGA). The catalytic activity was examined at 653 K and 6.0 MPa in a continuous fixed bed reactor for the hydrocracking (HCK) of model compounds of 1-methylnaphthalene (1-MN) and phenanthrene or a real feedstock of pyrolysis fuel oil (PFO). Overall, the Ni₂P/DS-β was observed as more active and stable in the hydrocracking of polycyclic aromatics than the Ni₂P/β catalyst. In addition, the Ni₂P/β suffered from the coke formation, while the Ni₂P/DS-β maintained the catalytic stability, particularly in the presence of large polycyclic hydrocarbons in the feed.

Keywords: Ni₂P; zeolite β; desilication; hydrocracking; polycyclic hydrocarbons; BTX

1. Introduction

Pyrolysis fuel oil (PFO), the by-product of naphtha cracking process, has been used as a low valued fuel oil as a heating source due to high content of polyaromatic hydrocarbon. In order to meet the increasing demand of engineering plastic (polyethylene, polypropylene), the conversion of PFO into benzene, toluene, xylenes (BTX) can be more beneficial for many petrochemical companies instead of building new naphtha cracking center. PFO is a mixture of alkyl-naphthalene, which can be converted into BTX by the hydrocracking process [1–3].

The hydrocracking process is known as the most effective process to convert polycyclic aromatics into BTX and distillates [4–6]. Most of the hydrocracking catalysts incorporate two functions of hydrogenation and cracking represented by a combination of a metal and an acidic support like silica-alumina or zeolites [7–10].

According to previous studies, NiMo/USY and NiW/USY catalysts exhibit good activity in hydrocracking reactions, but require high temperatures of around 773–1073 K and H₂ pressures of around 8.0–15.0 MPa. Besides, the catalysts tend to undergo rapid deactivation by coke formation on the strong acid sites in the zeolite [11–14]. Metal phosphides, as a novel hydroprocessing catalyst group, have been introduced [15–19], in which Ni₂P catalyst shows the best activity in hydroprocessing [16–29]. Our recent studies revealed that a Ni₂P supported on zeolite β shows a good activity in the hydrocracking of naphthalene and 1-methyl naphthalene at 673 K and 3.0–5.5 MPa [29,30], in which a bifunctional catalytic activity and inter-particulate porosity contribute to the high conversion. Considering

larger-sized polycyclic hydrocarbons in real feedstock, like pyrolysis fuel oils, the microporosity of zeolites can limit the diffusion of the molecules, causing coke formation. To lessen the diffusion limitation, desilication has been introduced to create mesoporosity within the zeolite structure [31], where Si can be selectively extracted from the zeolite framework in alkaline medium, typically NaOH [31–36]. Tarach et al. [36] confirmed the enhanced cracking activity of a mesoporous zeolite for gas–oils. Kenmogne et al. [37] demonstrated a bifunctional catalytic activity of a Pt/Al–MCM-48 in the hydrocracking of heavy oils.

This study focuses on Ni₂P catalysts supported on β zeolites to which desilication has been applied to obtain better accessibility toward acid sites. Moreover, pyrolysis fuel oils as a real feedstock were used in the feed for hydrocracking (HCK) over the Ni₂P/DS- β .

2. Results and Discussion

2.1. Characterization of Ni₂P Catalysts

The physical properties of the support and Ni₂P catalyst samples are given in Table 1. The Si/Al ratio was found to decrease from 12.66 to 10.47 after desilication of the zeolite β , indicating the removal of Si being achieved by the alkaline treatment. The Brunauer-Emmett-Teller (BET) surface area of the β and DS- β were 609.6 and 588.3 m²g⁻¹, respectively. The mesopore volume of the DS- β was much larger than that of parent β zeolite. These results indicate that the desilication increased the mesopore volume with little change of micropore volume. After the Ni₂P was loaded on the support, the BET surface area of Ni₂P/ β and Ni₂P/DS- β were 407.4 and 392.1 m²g⁻¹, respectively, due to a reduction in the pore volume with the loadings of Ni₂P. The spent samples of Ni₂P/ β underwent a significant reduction in the surface area due to the deposit of reaction products, including coke on the catalysts, resulting in the deactivation of the catalyst. Especially, in the presence of polyaromatic hydrocarbon such as phenanthrene, the micropore volume was almost blocked with the coke. This result indicates that the polyaromatic hydrocarbon compounds lead to coke formation during the HCK reaction. The amount of CO uptake for the spent samples was significantly reduced, indicating the loss of active sites, probably by the agglomeration of Ni₂P particles or coke deposits during the reaction. However, in the case of Ni₂P/DS- β , the amount of coke formation was lower than Ni₂P/ β . This result implies that the mesopore reduces the coke formation due to the enhanced accessibility of large aromatics towards active sites, resulting in a promotion of the hydrocracking activity. Furthermore, the mesopore in the desilicated β facilitates the accessibility of the reactants to the surface acid sites.

Table 1. Physical properties of the support and Ni₂P catalysts.

Samples	Conditions	BET Surface Area (m ² g ⁻¹)			Pore Volume (cm ³ g ⁻¹)		CO Uptake (μmol g ⁻¹)	Coke Formation ^d (wt.%)	Si/Al Ratio ^e
		S _{total}	S _{micro} ^a	S _{meso} ^b	V _{micro} ^a	V _{meso} ^c			
β	As calcined	609.6	484.2	125.3	0.24	0.39	-	-	12.66
DS- β	As calcined	588.3	347.4	240.9	0.15	0.77	-	-	10.47
Ni ₂ P/ β	Fresh	407.4	307.3	100.3	0.17	0.30	35.6	-	-
	Spent	110.7	34.8	75.9	0.01	0.25	10.7	14.2	-
Ni ₂ P/DS- β	Fresh	392.1	205.3	186.8	0.12	0.61	41.3	-	-
	Spent	261.5	87.1	174.4	0.06	0.58	32.8	5.7	-

^a Calculated by the *t*-plot method; ^b S_{total} – S_{micro}; ^c V_{total} – V_{micro}; ^d measured by thermogravimetric analysis (TGA) analysis; ^e measured by X-ray fluorescence (XRF) analysis.

Figure 1 shows the N₂ adsorption and desorption isotherms and the corresponding Barrett-Joyner-Halenda (BJH) pore size distribution for the β and DS- β samples. The parent β and DS- β showed type IV isotherms with an H3 hysteresis loop, indicating the existence of mesopores. The zeolite β is known to possess mesopores generated from the inter-particulate pore system [36].

It is notable that the DS- β increased the quantity of mesopore volume. Moreover, as shown in the pore size distribution in Figure 1, the mesopore distribution was remarkably developed (>10 nm).

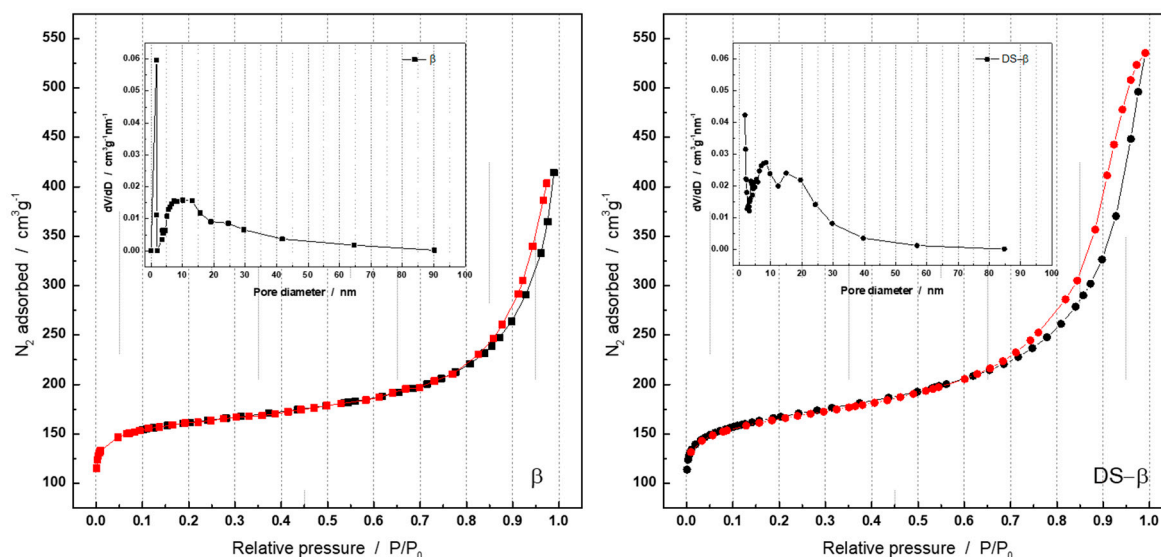


Figure 1. N_2 physisorption isotherms of β and DS- β .

Figure 2 shows the powder X-ray diffraction (XRD) patterns of the β and DS- β samples. The diffraction patterns for β and DS- β zeolite show main peak at 22.0° . The diffraction pattern of the DS- β shows that the β zeolite structure was mostly preserved, even after the desilication process, but with slightly being decreased in the crystallinity of the DS- β by 13% based on the diffraction peak intensity at 22.0° .

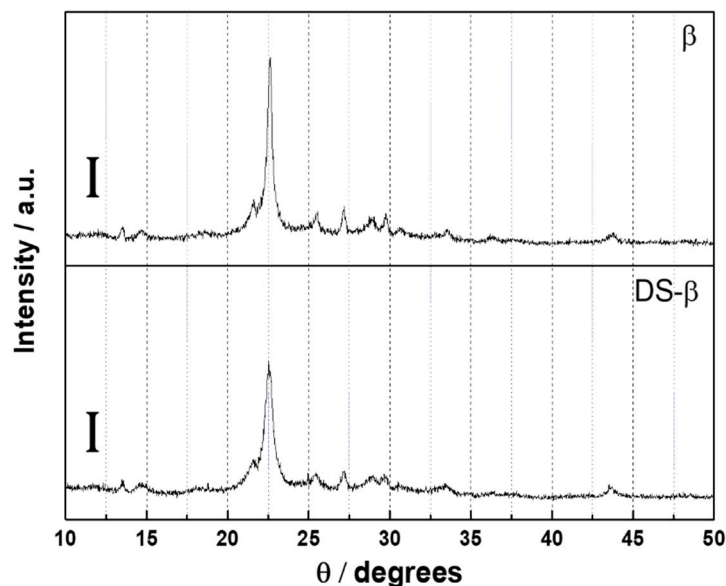


Figure 2. XRD patterns of β and DS- β .

The local coordinations of Al species in the β and DS- β samples were examined by solid-state ^{27}Al magic angle spinning–nuclear magnetic resonance (^{27}Al MAS NMR). Figure 3 displays the ^{27}Al MAS NMR spectra of the samples, exhibiting a strong peak at 57 ppm, corresponding to tetrahedral Al, and a weaker peak at 0 ppm to octahedral Al, which represents the Al species of in the framework (F-Al) and out of the framework (EF-Al), respectively [38–40]. For the samples, the peak areas were

calculated to obtain the relative amount of F-Al and EF-Al. After desilication, the F-Al content of desilicated β was decreased from 85 to 71% while the EF-Al content increased from 15 to 29%.

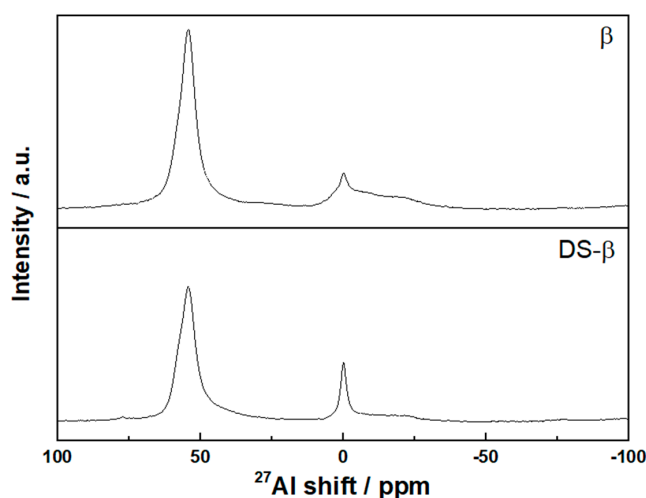


Figure 3. ^{27}Al magic angle spinning–nuclear magnetic resonance (^{27}Al MAS-NMR) spectra of β and DS- β .

Table 2 summarizes the acidity of the catalysts based upon the isopropyl amine temperature-programmed desorption (IPA-TPD) results. IPA-TPD measurements are useful to determine the strength and concentration of Brønsted acid sites. According to Gorte [41], Brønsted acid sites protonate amines to form alkylammonium ions that subsequently decompose to propene and ammonia above 575 K. Thus, desorption of propene indicates the presence of Brønsted sites. IPA-TPD profiles of the DS- β revealed that the propene desorption peak intensity slightly decreased, indicating the loss of Brønsted acid sites after the desilication process. After the nickel phosphide was loaded on the support by impregnation, the propene desorption peak intensities of $\text{Ni}_2\text{P}/\beta$ and $\text{Ni}_2\text{P}/\text{DS-}\beta$ were significantly reduced, due to the Ni_2P nanoparticles blocking the micropore volume. These results are well correlated with the BET results, as shown in Table 2. However, the propene desorption peak intensity of $\text{Ni}_2\text{P}/\text{DS-}\beta$ was higher than those of $\text{Ni}_2\text{P}/\beta$. These results imply that the $\text{Ni}_2\text{P}/\text{DS-}\beta$ catalyst retains larger porosity open to access for the reactants to better access the Brønsted acid sites. The total amount of acid sites and Brønsted acid sites were counted from the NH_3 -TPD and the IPA-TPD profiles, respectively. The amount of Brønsted acid sites of the DS- β was slightly lower than parent β zeolite, indicating the loss of FAL species during the desilication process [35]. These results are well correlated with the XRD and ^{27}Al -MAS NMR results, as shown in Figures 2 and 3. On the other hand, the amount of Brønsted acid sites of $\text{Ni}_2\text{P}/\text{DS-}\beta$ was higher than $\text{Ni}_2\text{P}/\beta$. These results imply that the $\text{Ni}_2\text{P}/\text{DS-}\beta$ catalyst provides better accessibility of the reactants toward the Brønsted acid sites.

Table 2. Acidic properties of the β and DS- β zeolites.

Samples	Amount of Total Acid Sites ^a ($\mu\text{mol g}^{-1}$)	Amount of Brønsted Acid Sites ^b ($\mu\text{mol g}^{-1}$)	Fraction of Brønsted Acid Site ^c (%)
β	710.0	315.0	48
DS- β	630.6	283.7	45
$\text{Ni}_2\text{P}/\beta$	380.6	67.9	18
$\text{Ni}_2\text{P}/\text{DS-}\beta$	517.2	113.0	22

^a The total acidity was determined by quantifying the desorbed NH_3 using NH_3 -TPD. ^b The Brønsted acidity was determined by quantifying the desorbed propylene using isopropyl amine temperature-programmed desorption (IPA-TPD). ^c The ratio of the amount of Brønsted acid sites to the total amount of acid sites.

Figure 4 displays the Ni K-edge extended X-ray absorption fine structure (EXAFS) spectra for the Ni_2P catalysts and bulk Ni_2P reference sample. The spectrum for Ni_2P exhibits a wider oscillation region in $30.0\text{--}80.0\text{ nm}^{-1}$ corresponding to Ni–P contribution and a narrower oscillation region in $80.0\text{--}140.0\text{ nm}^{-1}$ for Ni–Ni contribution, generating two distinct peaks in the Fourier transforms (FT), centered at 0.175 nm and 0.240 nm for Ni–P and Ni–Ni shells, respectively [42]. The zeolite-supported Ni_2P catalysts also exhibit the similar FT profiles as those of the bulk Ni_2P reference, implying the formation of Ni_2P phase on the β and DS- β . The spent Ni_2P samples also exhibit very similar spectra with only a slight decrease in Ni–Ni peak intensity of Fourier transforms, indicating that the Ni_2P phase is mostly maintained during the reaction.

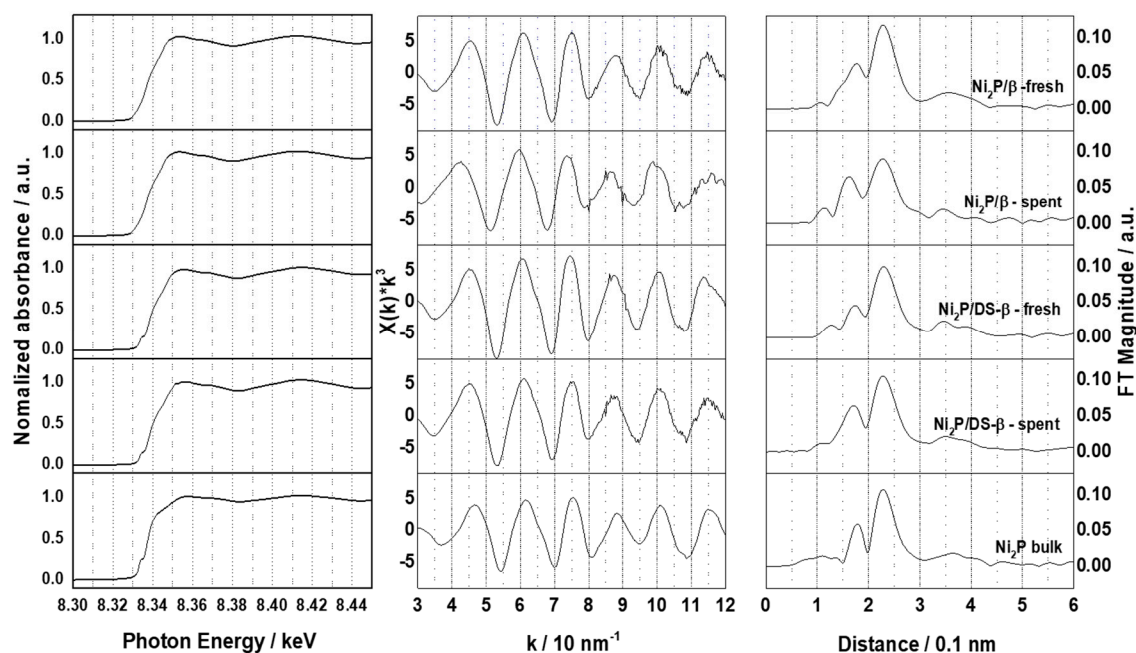


Figure 4. Ni K-edge extended X-ray absorption fine structure (EXAFS) spectra for the fresh and spent Ni_2P catalysts and bulk Ni_2P samples.

2.2. Hydrocracking Activity of Ni_2P Catalysts

Figure 5 shows the conversion, 1-ring aromatics (1-Ar), and BTX yields of the hydrocracking of polycyclic aromatics over the Ni_2P catalysts at 653 K , 6.0 MPa , and liquid hourly space velocity (LHSV) of 1.0 h^{-1} . The $\text{Ni}_2\text{P}/\text{DS-}\beta$ also exhibited very high and stable conversion of 1-methylnaphthalene (1-MN, 2-Ar) over 98%, even in the presence of phenanthrene (3-Ar) with high and stable BTX yield of 43.1 wt.%, while the $\text{Ni}_2\text{P}/\beta$ gave relatively low 2-Ar and 3-Ar conversion below 55%. These results suggest that the coke deposition was accelerated on the catalyst surface, leading to the agglomeration of Ni_2P particles and reduced exposed acid sites, as evident from the CO uptake and thermogravimetric analysis (TGA) summarized in Table 2. Moreover, the $\text{Ni}_2\text{P}/\text{DS-}\beta$ catalyst exhibited higher BTX yield than the $\text{Ni}_2\text{P}/\beta$ catalyst at the same reaction conditions in presence of 3-ring polycyclic aromatics. These results indicate that the catalytic activity for hydrocracking of polycyclic aromatics depends on both the concentration of acid sites and the accessibility toward the acid sites.

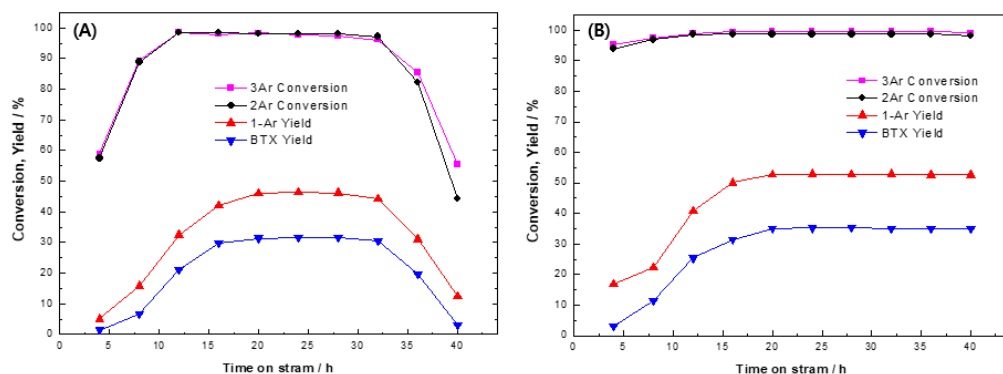


Figure 5. Hydrocracking (HCK) performances for 1-methylnaphthalene and phenanthrene over Ni₂P/β (A) and Ni₂P/DS-β (B) at 653 K and 6.0 MPa.

Figure 6 shows the 1-Ar and BTX yields of the hydrocracking of PFO over the Ni₂P catalysts at 653 K, 6.0 MPa, and LHSV of 1.0 h⁻¹. Similarly, the Ni₂P/β exhibited high 1-Ar and BTX yield of 46.3 and 31.6 wt.% at the steady-state condition, but a gradual decrease of BTX yield was observed over the Ni₂P/β catalyst, especially over 168 h of reaction, suggesting that a coke deposit might occur on the Ni₂P/β catalyst with causing a loss in cracking activity. In contrast, the Ni₂P/DS-β exhibited high and stable HCK activity with 1-Ar and BTX yields of 52.7 and 35.1 wt.%, respectively. Therefore, these results demonstrate that the desilication of the zeolite supports plays a crucial role in the hydrocracking of PFO into BTX with providing better accessibility toward active centers, leading to enhanced stability toward 2- or 3-Ar enriched feedstocks.

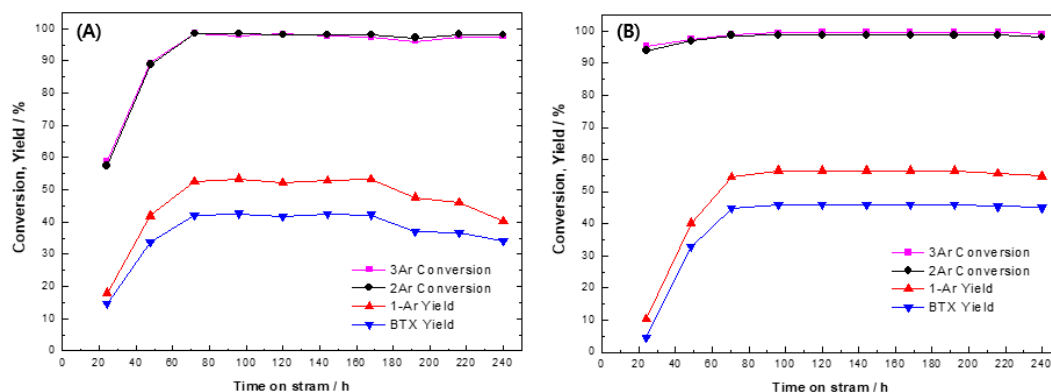


Figure 6. HCK performances for pyrolysis fuel oil (PFO) over Ni₂P/β (A) and Ni₂P/DS-β (B) at 653 K and 6.0 MPa.

3. Experimental

3.1. Materials and Catalysts Preparation

Model compounds of 1-methylnaphthalene (Alfa Aesar, Haverhill, MA, USA, 98%) and phenanthrene (Aldrich, Montgomery, AL, USA, 95%) were used as received. The PFO feed was supplied from Hanwha Total petrochemical company in Seosan, Korea, and the specification is given in Table 3. PFO fractions of boiling temperature below 573 K are composed mainly of alkyl-derivate naphthalenes, which were easy to produce BTX through hydrocracking process. Commercial zeolite (β, CP814E, SiO₂/Al₂O₃ = 25) was obtained from Zeolyst. Desilication was carried out using alkaline treatment as reported in literature [11]. Zeolite β (5 g) sample was treated with NaOH aqueous solution (300 mL, 0.2 M, 363 K, 30 min) with tetrapropylammonium bromide (0.2 M), as a pore directing agent (PDA). The sample was then filtrated, thoroughly washed with deionized water, and dried at 393 K overnight, followed by calcined at 773 K in air for 5 h to remove organic material. The calcined sample was converted to ammonium forms by three times ion-exchange (0.2 M NH₄NO₃, 363 K, 1 h). Then,

the obtained sample was calcined in air at 773 K for 5 h, to obtain the H-forms, which was denoted as DS- β .

Table 3. The composition of pyrolysis fuel oil (PFO).

Physical Properties		PFO
	C (wt.%)	87.5
	H (wt.%)	9.0
	S/ppm	70
	N/ppm	-
	Total	77.6
Aromatics/wt.%	Mono	31.1
	Di	43.0
	Tri+	3.5
Distillation/K	IBP/5/10	343/388/408/
	30/40/50	448/488/538/
	60/90/95/EP	593/848/873/-

The loading amount of Ni was 1.5 mmol g⁻¹ of support with the initial Ni/P ratio in the precursors of 0.5. The oxidic precursors were obtained by incipient wetness impregnation of the supports with a solution of Ni(NO₃)₂·6H₂O (Alfa Aesar, Haverhill, MA, USA) and (NH₄)₂HPO₄ (Samchun, Seoul, Korea), and the mixture was dried at 393 K for 7 h and calcined at 673 K for 6 h. The calcined materials were reduced at 873 K in quartz U-tube reactors under 1000 mol H₂ s⁻¹ (1500 cm³ (NTP) min⁻¹) per gram of sample. After reduction, the catalyst samples were cooled down to room temperature in He flow, followed by passivation in 0.2% O₂/He flow for 4 h.

3.2. Catalyst Characterization

N₂ isotherms of the catalyst samples were measured on Micromeritics ASAP 2060. The specific surface area was obtained from the linear portion of BET plots ($P/P_0 = 0.01-0.10$) at 77 K. The pore size distribution was obtained from the desorption branch of the isotherm following the BJH method. The XRD patterns of the samples were obtained using a diffractometer (Rigaku DMAX-2500) operated at 60 kV and 300 mA with Cu K α radiation ($\lambda = 0.15418$ nm). The X-ray fluorescence (XRF) measurements were used to determine the Si/Al molar ratio of the zeolite samples with a Shimadzu XRF-1700 sequential XRF spectrometer at 30 mA and 40 kV. CO uptake measurements were conducted at room temperature using pulses (100 μ L) of CO on the passivated and air-exposed samples re-reduced in H₂ at 723 K for 2 h. Ammonia and isopropyl amine (IPA) temperature-programmed desorption (TPD) measurements were conducted to determine the acidity of the catalysts. For TPD measurements, 0.1 g of the sample was pretreated in He for 2 h at 723 K, and then cooled to 373 K. For NH₃-TPD, the sample was exposed to 1 vol% NH₃ in a He flow of 100 cm³ min⁻¹ at 373 K until saturation, whereas for IPA-TPD, it was exposed to 5 vol% IPA in a He flow of 100 cm³ min⁻¹ at 373 K until saturation. During the adsorption the effluent from the reactor was sampled into a mass spectrometer (HP 5973N inert) to monitor species. After then, the reactor was heated to 1073 K at a ramping rate of 10 K min⁻¹. Again, the effluent gas was monitored by the mass spectrometer during the heating. Thermogravimetric analysis (SDT2960, TA instruments) was conducted to measure the amounts of the coke on the spent Ni₂P catalysts after reaction tests. ²⁷Al Magic Angle Spinning–Nuclear Magnetic Resonance (²⁷Al MAS NMR) were measured with a Bruker Avance III HD 500 NMR spectrometer using a 4-mm triple-resonance probe head at the resonance frequency of 130.3 MHz, the pulse length of 2 μ s, and the spinning speed of 10 kHz. An Al reference of (NH₄)Al(SO₄)₂·12H₂O was used as the ²⁷Al chemical shifts. The Ni K edge X-ray absorption spectra of the catalyst samples were obtained at the beamlines 8C and 10C of the Pohang Light Source (PLS).

3.3. Activity Tests for Hydrocracking of Polycyclic Aromatic Hydrocarbons and PFO

Hydrocracking tests were performed at 653 K and 6.0 MPa in a continuous fixed bed reactor with a model feed mixture including 2- to 3-Ar or pyrolysis fuel oils. The model feed mixture was obtained by mixing 20 wt.% phenanthrene (Aldrich, Montgomery, AL, USA, 95%) in 1-methylnaphthalene (Alfa Aesar, Haverhill, MA, USA, 98%). The feed mixture was fed at $0.017 \text{ cm}^3 \text{ min}^{-1}$ using a liquid pump (Laballiance series II, Selangor, Malaysia) with a He flow of $100 \text{ cm}^3 \text{ min}^{-1}$. The Ni_2P catalysts of 1.0 cm^3 were loaded and the liquid hourly space velocity (LHSV) was 1.0 h^{-1} . The products were quantified using a GC (Agilent 6890, Santa Clara, CA, USA), equipped with a dimethylsiloxane column (Hewlett Packard, HP-1, 30 m, 0.32 mm i.d.), on samples collected at 3–4 h intervals. Conversions and yields of the model compounds and BTX products were defined as Equations (1)–(4).

$$2\text{Ar conversion (wt.\%)} = \frac{1\text{MN}_{\text{initial}} - 1\text{MN}_{\text{final}}}{1\text{MN}_{\text{initial}}} \times 100 \quad (1)$$

$$3\text{Ar conversion (wt.\%)} = \frac{\text{Phe}_{\text{initial}} - \text{Phe}_{\text{final}}}{\text{Phe}_{\text{initial}}} \times 100 \quad (2)$$

$$\text{BTX yield (wt.\%)} = \frac{\text{Benzene} + \text{Toluene} + \text{Xylenes}}{1\text{MN}_{\text{initial}} + \text{Phe}_{\text{initial}}} \times 100 \quad (3)$$

$$1\text{Ar yield (wt.\%)} = \frac{\text{BTX} + (\text{ethyl} + \text{propyl} + \text{butyl})\text{Benzene}}{1\text{MN}_{\text{initial}} + \text{Phe}_{\text{initial}}} \times 100 \quad (4)$$

4. Conclusions

The effects of desilication of β zeolite (DS- β) on the formation of mesoporosity were studied using Ni_2P supported on β or desilicated β for the hydrocracking polycyclic hydrocarbons at 6.0 MPa and 653 K in a fixed bed reactor. The $\text{Ni}_2\text{P}/\text{DS-}\beta$ exhibited more active and stable behavior for the hydrocracking of polycyclic aromatics than the $\text{Ni}_2\text{P}/\beta$. It was noted that the DS- β had well-developed intra-mesopores with better dispersion of Ni_2P catalysts and more accessible acid sites, leading to remarkable activity in the hydrocracking of polycyclic aromatics. In contrast, the $\text{Ni}_2\text{P}/\beta$ underwent deactivation by coke formation in the presence of 3-Ar in the feed. Thus, it can be suggested that the desilicated β -supported Ni_2P catalyst can be a good hydrocracking catalyst for converting polycyclic aromatics into value-added light aromatic compounds.

Author Contributions: Y.-K.L. conceived and designed the experiments; Y.-S.K. and K.-S.C. performed the experiments; Y.-S.K. and Y.-K.L. wrote the paper. All authors have read and agreed to the published version of the manuscript.

Funding: This research received no external funding.

Acknowledgments: This research was funded by Dankook University in 2017.

Conflicts of Interest: The authors declare no conflict of interest.

References

1. Mayani, V.J.; Mayani, S.V.; Lee, Y.; Park, S.-K. A non-chromatographic method for the separation of highly pure naphthalene crystals from pyrolysis fuel oil. *Sep. Purif. Technol.* **2011**, *80*, 90–95. [[CrossRef](#)]
2. Khani, M.R.; Guy, E.D.; Gharibi, M.; Shahabi, S.S.; Khosravi, A.; Norouzi, A.A.; Shokri, B. The effects of microwave plasma torch on the cracking of Pyrolysis Fuel Oil feedstock. *Chem. Eng. J.* **2014**, *237*, 169–175. [[CrossRef](#)]
3. Kim, J.G.; Liu, F.; Lee, C.-W.; Lee, Y.-S.; Im, J.S. Boron-doped carbon prepared from PFO as a lithium-ion battery anode. *Solid State Sci.* **2014**, *34*, 38–42. [[CrossRef](#)]
4. Ishihara, A.; Itoh, T.; Nasu, H.; Hashimoto, T.; Doi, T. Hydrocracking of 1-methylnaphthalene/decahydronaphthalene mixture catalyzed by zeolite-alumina composite supported NiMo catalysts. *Fuel Process. Technol.* **2013**, *116*, 222–227. [[CrossRef](#)]

5. Park, J.I.; Lee, J.K.; Miyawaki, J.; Kim, Y.K.; Yoon, S.H.; Mochida, I. Hydro-conversion of 1-methyl naphthalene into (alkyl)benzenes over alumina-coated USY zeolite-supported NiMoS catalysts. *Fuel* **2011**, *90*, 182–189. [[CrossRef](#)]
6. Lapinas, A.T.; Klein, M.T.; Gates, B.C.; Macris, A.; Lyons, J.E. Catalytic hydrogenation and hydrocracking of fluorene: Reaction pathways, kinetics, and mechanisms. *Ind. Eng. Chem. Res.* **1991**, *30*, 42–50. [[CrossRef](#)]
7. Ward, J.W. Hydrocracking processes and catalysts. *Fuel Process. Technol.* **1993**, *35*, 55–85. [[CrossRef](#)]
8. Weitkamp, J. Isomerization and hydrocracking of C₉ through C₁₆ n-alkanes on Pt/HZSM-5 zeolite. *Appl. Catal.* **1983**, *8*, 123–141. [[CrossRef](#)]
9. Martens, J.A.; Jacobs, P.A.; Weitkamp, J. Attempts to rationalize the distribution of hydrocracked products. I. qualitative description of the primary hydrocracking modes of long chain paraffins in open zeolites. *Appl. Catal.* **1986**, *20*, 239–281. [[CrossRef](#)]
10. Martens, J.A.; Jacobs, P.A.; Weitkamp, J. Attempts to rationalize the distribution of hydrocracked products. II. Relative rates of primary hydrocracking modes of long chain paraffins in open zeolites. *Appl. Catal.* **1986**, *20*, 283–303. [[CrossRef](#)]
11. Dufresne, P.; Quesada, A.; Mignard, S. Influence of nitrogen feed content on the performances of A zeolite hydrocracking catalyst. *Stud. Surf. Sci. Catal.* **1990**, *53*, 301–315.
12. Leglise, J.; Manoli, J.M.; Potvin, C.; Djega-Mariadassou, G.; Cornet, D. The nature of NiMo phases engaged in HY zeolites. *J. Catal.* **1995**, *152*, 275–290. [[CrossRef](#)]
13. Cid, R.; Neira, J.; Godoy, J.; Palacios, J.M.; Lopez Agudo, A. Thiophene hydrodesulfurization on sulfided nickel exchanged USY zeolites. Effect of the pH of the catalyst preparation. *Appl. Catal. A Gen.* **1995**, *125*, 169–183. [[CrossRef](#)]
14. Welters, W.J.J.; Vorbeck, G.; Zandbergen, H.W.; de Haan, J.W.; de Beer, V.H.J.; van Santen, R.A. HDS activity and characterization of zeolite-supported nickel sulfide catalysts. *J. Catal.* **1994**, *150*, 155–169. [[CrossRef](#)]
15. Korányi, T.I. Phosphorus promotion of Ni (Co)-containing Mo-free catalysts in thiophene hydrodesulfurization. *Appl. Catal. A Gen.* **2003**, *239*, 253–267. [[CrossRef](#)]
16. Stinner, C.; Tang, Z.; Haouas, M.; Weber, T.; Prins, R. Preparation and P-31 NMR characterization of nickel phosphides on silica. *J. Catal.* **2002**, *208*, 456–466. [[CrossRef](#)]
17. Deliy, I.V.; Shamanaev, I.V.; Aleksandrov, P.V.; Gerasimov, E.Y.; Pakharukova, V.P.; Kodenev, E.G.; Yakovlev, I.V.; Lapina, O.B.; Bukhtiyarova, G.A. Support Effect on the Performance of Ni₂P Catalysts in the Hydrodeoxygenation of Methyl Palmitate. *Catalysts* **2018**, *8*, 515. [[CrossRef](#)]
18. Jang, J.-G.; Lee, Y.-K. Promotional Effect of Ga for Ni₂P Catalyst on Hydrodesulfurization of 4,6-DMDBT. *Appl. Catal. B Environ.* **2019**, *250*, 181–188. [[CrossRef](#)]
19. Yun, G.-N.; Cho, K.-S.; Kim, Y.-S.; Lee, Y.-K. A New Approach to Deep Desulfurization of Light Cycle Oil over Ni₂P Catalysts: Combined Selective Oxidation and Hydrotreating. *Catalysts* **2018**, *8*, 102.
20. Yun, G.-N.; Lee, Y.-K. Dispersion Effects of Ni₂P Catalysts on Hydrotreating of Light Cycle Oil. *Appl. Catal. B Environ.* **2014**, *150*, 647–655. [[CrossRef](#)]
21. Lee, Y.-K.; Oyama, S.T. Sulfur Resistant Nature of Ni₂P Catalyst in Deep Hydrodesulfurization. *Appl. Catal. A Gen.* **2017**, *548*, 103–113. [[CrossRef](#)]
22. Cho, K.-S.; Seo, H.-R.; Lee, Y.-K. A New Synthesis of Highly Active Ni₂P/Al₂O₃ Catalyst by Liquid Phase Phosphidation for Deep Hydrodesulfurization. *Catal. Commun.* **2011**, *12*, 470–474. [[CrossRef](#)]
23. Cho, K.-S.; Kim, S.-H.; Lee, Y.-K. XAFS Studies on Highly Dispersed Ni₂P/SiO₂ Catalysts for Hydrodesulfurization of 4,6-Dimethyldibenzothiophene. *Nucl. Instrum. Methods Phys. Res. A* **2010**, *621*, 690–694. [[CrossRef](#)]
24. Cho, K.-S.; Seo, H.-R.; Kim, S.-H.; Lee, Y.-K. Nickel Phosphide Catalysts Supported on SBA-15 for the Hydrodesulfurization of 4,6-DMDBT. *J. Jpn. Petrol. Inst.* **2010**, *53*, 173–177. [[CrossRef](#)]
25. Oyama, S.T.; Gott, T.; Zhao, H.; Lee, Y.-K. Transition metal phosphide hydroprocessing catalysts: A review. *Catal. Today* **2009**, *143*, 94–107. [[CrossRef](#)]
26. Lee, Y.-K.; Shu, Y.; Oyama, S.T. Active Phase of a Nickel Phosphide (Ni₂P) Catalyst Supported on KUSY Zeolite for the Hydrodesulfurization of 4,6-DMDBT. *Appl. Catal. A Gen.* **2007**, *322*, 191. [[CrossRef](#)]
27. Oyama, S.T.; Lee, Y.-K. Mechanism of Hydrodenitrogenation on Phosphides and Sulfides. *J. Phys. Chem. B* **2005**, *109*, 2109–2119. [[CrossRef](#)]
28. Oyama, S.T.; Wang, X.; Lee, Y.-K.; Bando, K.; Requejo, F.G. Effect of phosphorus content in nickel phosphide catalysts studied by XAFS and Other Techniques. *J. Catal.* **2002**, *210*, 207–217. [[CrossRef](#)]

29. Kim, Y.-S.; Yun, G.-N.; Lee, Y.-K. Novel Ni₂P/zeolite catalysts for naphthalene hydrocracking to BTX. *Catal. Commun.* **2014**, *45*, 133–138. [[CrossRef](#)]
30. Kim, Y.-S.; Cho, K.-S.; Lee, Y.-K. Morphology effect of β -zeolite supports for Ni₂P catalysts on the hydrocracking of polycyclic aromatic hydrocarbons to benzene, toluene, and xylene. *J. Catal.* **2017**, *351*, 67–78. [[CrossRef](#)]
31. You, S.J.; Park, E.D. Effects of dealumination and desilication of H-ZSM-5 on xylose dehydration. *Micropor. Mesopor. Mater.* **2014**, *186*, 121–129. [[CrossRef](#)]
32. Rac, V.; Rakic, V.; Stosic, D.; Otaman, O.; Auroux, A. Hierarchical ZSM-5, Beta and USY zeolites: Acidity assessment by gas and aqueous phase calorimetry and catalytic activity in fructose dehydration reaction. *Micropor. Mesopor. Mater.* **2014**, *194*, 126–134. [[CrossRef](#)]
33. Mlekodaj, K.; Tarach, K.; Datka, J.; Gora-Marek, K.; Makowski, W. Porosity and accessibility of acid sites in desilicated ZSM-5 zeolites studied using adsorption of probe molecules. *Micropor. Mesopor. Mater.* **2014**, *183*, 54–61. [[CrossRef](#)]
34. Sadowska, K.; Gora-Marek, K.; Datka, J. Hierarchic zeolites studied by IR spectroscopy: Acid properties of zeolite ZSM-5 desilicated with NaOH and NaOH/tetrabutylamine hydroxide. *Vib. Spectrosc.* **2012**, *63*, 418–425. [[CrossRef](#)]
35. Zhu, X.; Lobban, L.L.; Mallinson, R.G.; Resasco, D.E. Tailoring the mesopore structure of HZSM-5 to control product distribution in the conversion of propanal. *J. Catal.* **2010**, *271*, 88–98. [[CrossRef](#)]
36. Tarach, K.; Góra-Marek, K.; Tekla, J.; Brylewska, K.; Datka, J.; Mlekodaj, K.; Makowski, W.; Igualada López, M.C.; Martínez Triguero, J.; Rey, F. Catalytic cracking performance of alkaline-treated zeolite Beta in the terms of acid sites properties and their accessibility. *J. Catal.* **2014**, *312*, 46–57. [[CrossRef](#)]
37. Kenmogne, R.; Finiels, A.; Cammarano, C.; Hulea, V.; Fajula, F. Hydroconversion of n-hexadecane over bifunctional microporous and mesoporous model catalysts. Influence of pore architecture on selectivity. *J. Catal.* **2015**, *329*, 348–354. [[CrossRef](#)]
38. Gackowski, M.; Taracz, K.; Kuterasiński, L.; Podobiński, J.; Sulikowski, B.; Datka, J. Spectroscopic IR and NMR studies of hierarchical zeolites obtained by desilication of zeolite Y: Optimization of the desilication route. *Micropor. Mesopor. Mater.* **2019**, *281*, 134–141. [[CrossRef](#)]
39. Haouas, M.; Taulelle, F.; Martineau, C. Recent advances in application of ²⁷Al NMR spectroscopy to materials science. *Prog. Nucl. Magn. Reson. Spectrosc.* **2016**, *94–95*, 11–36. [[CrossRef](#)]
40. Sazama, P.; Tabor, E.; Klein, P.; Wichterlova, B.; Sklenak, S.; Mokrzycki, L.; Pashkova, V.; Ogura, M.; Dedecek, J. Al-rich beta zeolites. Distribution of Al atoms in the framework and related protonic and metal-ion species. *J. Catal.* **2016**, *333*, 102–114. [[CrossRef](#)]
41. Gorte, R.J. What do we know about the acidity of solid acids? *Catal. Lett.* **1999**, *62*, 1–13. [[CrossRef](#)]
42. Lee, Y.-K.; Oyama, S.T. Bifunctional nature of a SiO₂-supported Ni₂P catalyst for hydrotreating: EXAFS and FTIR studies. *J. Catal.* **2006**, *239*, 376–389. [[CrossRef](#)]

